scientific reports

Check for updates

OPEN

Waveform cross-correlation analysis and magnitude estimation for the 1887 Ligurian earthquake determined from magnetogram recordings

Gabriele Tarchini[1]✉, Stefano Parolai[2], Daniele Spallarossa[1] & Denis Sandron[3]

The Ligurian earthquake of 23 February 1887, one of the most significant historical earthquakes in southwestern Europe, is re-evaluated in this study through the analysis of digitized records from 19th-century magnetometers. Traces from the magnetic observatories in Greenwich, Kew, Falmouth (UK) and Paris Saint-Maur (France) were retrieved and digitized to identify disturbances caused by the earthquake ground motion. Synthetic seismograms were generated using full-wavefield modeling and then convolved with the transfer function of classical magnetometers to simulate the expected responses. A cross-correlation analysis between observed and synthetic traces was performed to assess the consistency of different fault-plane scenarios. The results support the plausibility of a low-angle, north-dipping reverse fault as the source mechanism, which is consistent with tsunami modeling results and regional tectonic constraints. A comparative approach with a recent, well-recorded reference earthquake was used to estimate the moment magnitude of the 1887 event based on magnetogram amplitudes. This highlights the potential of historical magnetograms to contribute to the quantitative reassessment of major pre-instrumental events and provides valuable insights for seismic hazard assessment.

The "Ligurian" earthquake of 23 February 1887 is one of the most significant and devastating earthquakes known to have occurred in the southwestern Alps–Ligurian Basin junction (Italy, France) during the last millennium[1–3]. It was the first and strongest of a series of three shocks of destructive violence that caused extensive damage along the coast (where a tsunami also occurred) and inland from Nice (France) to beyond Savona (Italy). The damage caused by the earthquakes included at least 600 deaths and the destruction of many buildings, causing around 20,000 people to lose their homes[4]. The structural weaknesses of the buildings (such as inadequate reinforcements, excessive height in relation to wall thickness, and the use of poor materials), pre-existing damage from previous earthquakes (the last of which occurred in 1854) and the fact that the mainshock occurred shortly after six o'clock on the morning of Ash Wednesday probably contributed to the high death toll[5].

Due to its long and complex geological history, largely dominated by the convergence between the African and Eurasiatic plates and the subduction rollback of the Tethys Ocean beneath the Apennines[6–8], the southwestern Alps–Ligurian Basin junction represents an area of considerable topographic and structural complexity, characterized by significant tectonic and topographic heritage and accumulated deformation. This region is characterized by ENE–WSW step-fault systems and NNW–SSE faults that cut across the continental margin and represent the offshore continuation of strike-slip faults and grabens found inland[9]. The region is characterized by continuous low-to-moderate seismic activity and is one of the most seismically active areas in western Europe[10–17]. The distribution of seismicity—which extends over a large area, both onshore and offshore, with generally shallow focal depths (~5–20 km)—is primarily diffuse[16,18], although low-magnitude earthquakes tend to cluster along the ENE–WSW trending fault systems and often exhibit predominantly compressional and transpressional focal mechanisms[18–20]. In contrast, extensional tectonic activity occurs mainly along the upper continental slope, characterized by significant sedimentation and a complex system of canyons that incise the continental slope more or less perpendicularly[21].

[1]Department of Earth, Environmental and Life Sciences, University of Genoa, 16132 Genoa, Italy. [2]Department of Mathematics, Informatics and Geosciences, University of Trieste, 34128 Trieste, Italy. [3]National Institute of Oceanography and Applied Geophysics, OGS, 34128 Trieste, Italy. ✉email: gabriele.tarchini@edu.unige.it

Despite its low deformation rates, this area has experienced notable historical earthquakes, including the 1564 "Nissart" earthquake (macroseismic intensity, I ~VIII on the Mercalli–Cancani–Sieberg scale), the 1887 Ligurian earthquake (I ~IX on the Medvedev–Sponheuer–Karnik scale) and, more recently, an M_L (local magnitude) 6.0 earthquake in 1963[22]. Strong pre-instrumental earthquakes provide valuable information to better understand regional seismicity, tectonic processes, and the seismic potential of areas with moderate seismic activity and complex geology. This knowledge can be crucial to gain insights into the associated deformation zones and has strong implications for probabilistic seismic hazard analysis[23,24]. However, the investigation of historical earthquakes—particularly in terms of quantitative re-evaluation of their source parameters—can be challenging. The 1887 Ligurian earthquake exemplifies such difficulties, as its precise epicenter (offshore versus onshore), moment magnitude (currently estimated between 6.3 and 7.5 M_w), and focal mechanism are difficult to characterize with a high degree of precision and have been disputed for years[1,16,25–29]. The accurate characterization of the 1887 Ligurian earthquake assumes an even greater significance considering that this event was selected by the Italian Civil Protection Department as the main earthquake for the definition of deterministic ground shaking scenarios for western Liguria[30], with strong implications on seismic classification and seismic hazard assessment.

A re-evaluation of the 1887 Ligurian earthquake by Larroque et al. in 2012 used information from the French and Italian macroseismic databases (DBMI15[31]; SISFRANCE[32]), updated intensity prediction equations[33], and structural and bathymetric data collected during the MALISAR geophysical survey[34]. According to their results, the macroseismic epicenter of the event was located offshore, approximately $43.70^\circ - 43.78^\circ$ N and $7.81^\circ - 8.07^\circ$ E. They suggested that a reverse 235°-striking fault plane dipping 16° to the north is the most consistent scenario to account for the 1887 Ligurian earthquake and to explain the characteristics of the subsequent tsunami[22]. In addition to instrumental recordings of tide gauges in the harbors of Genoa (Italy) and Nice, and of a Cecchi seismograph in Moncalieri (Italy)[35–38]—which, despite its historical relevance, was probably unreliable as it only recorded the east-west component, although it was located in an area of strong ground shaking[39]—several magnetic observatories throughout Europe also recorded the Ligurian earthquake[4]. These observatories were equipped with magnetometers, which were primarily used to measure the direction, strength, and fluctuations of the Earth's magnetic field. However, these instruments could also detect seismic waves, which were essentially disturbances[40–43], albeit with a magnification much lower than the sensitivity threshold of most seismometers[42,44]. Although some early authors[45] interpreted the magnetogram disturbances caused by the Ligurian earthquake as possible effects of transient electric currents induced during the event, later analyses[4,42,46] rejected this hypothesis. In particular, the inconsistencies in the arrival times at different stations and the fact that not all magnetic instruments at a particular location recorded the disturbances suggested a mechanical rather than an electromagnetic origin. Specifically, a close examination of the 23 February 1887 magnetograms recorded with identical instruments at the French observatories of Perpignan, Lyon, and Paris Saint-Maur led Poirier et al. to conclude that, although the signals superficially resembled the time stamps of electrical pulses, the characteristics of the observed oscillations differed in subtle but significant ways[47] (i.e., longer duration and excitation patterns consistent with the free oscillation of the magnetic bars). These results suggest that the magnetometers were indeed set in motion by the passage of seismic waves and essentially behaved like rudimentary horizontal pendulum seismometers. We therefore interpret the perturbations observed on the magnetograms as genuine ground-motion signals associated with the Ligurian earthquake, rather than electromagnetic artifacts. This is further corroborated by an original annotation on the magnetograms recorded in Greenwich that explicitly attributes the recorded disturbances to the mainshock on the Ligurian coast (Fig. 1).

Almost uninterrupted magnetometer records are kept by the British Geological Survey (BGS) (https://www.bgs.ac.uk/) and the Bureau Central de Magnétisme Terrestre (BCMT) (http://www.bcmt.fr/). In particular, we were able to retrieve the magnetic horizontal-force (H) and declination (D) traces recorded at the observatories in Greenwich, Kew, Falmouth (UK) and Paris Saint-Maur (France) (Fig. 2) in the form of scanned images. As an example, Fig. 1 shows the traces recorded at the Greenwich magnetic observatory, in which the identification of earthquake-induced disturbances is clear. The scanned records of the other observatories can be found in Figs. S1–S3 in the Supplementary Information.

Seismo-magnetic data

In 1846, at the Royal Greenwich magnetic observatory, in Great Britain, absolute determinations of the various components of the geomagnetic field started to be carried out continuously using Gauss's method applied to magnetometers[48–50]. This method employed photographic paper attached to a slowly rotating drum to record a beam of light reflected from a set of mirrors, one of which attached to a moving bar magnet inside the instrument, which had to be permanently placed in a dark and thermally-stable site. Over the following decades, other observatories joined in the continuous recording of magnetic data.

An impressively extensive data set of more than 160 years of continuous measurements in the UK was scanned and made available in 2009 as part of the "OpenGeoscience" project of the BGS.

The yearbooks issued by the BGS[51] provide details on the magnetometers, their measurements, and technical specifications regarding the response of the instruments to seismic waves. At Greenwich, they record several changes in the position of the instruments, mainly aimed at improving temperature stability. A change in the photographic paper in 1882 is also noted, while the instrumentation then remained unmodified until the installation of new magnetometers in 1915. The instruments installed in Falmouth and Kew were of the same basic design as in Greenwich. For Falmouth, no changes are reported between 1894 and 1910, while at Kew the magnetometers were installed in 1857 and left unchanged until 1911. At Paris Saint-Maur, continuous recordings started in 1883 with a Mascart variometer; this instrument did not substantially differ from those installed in the UK, and its response to seismic waves can therefore be considered comparable.

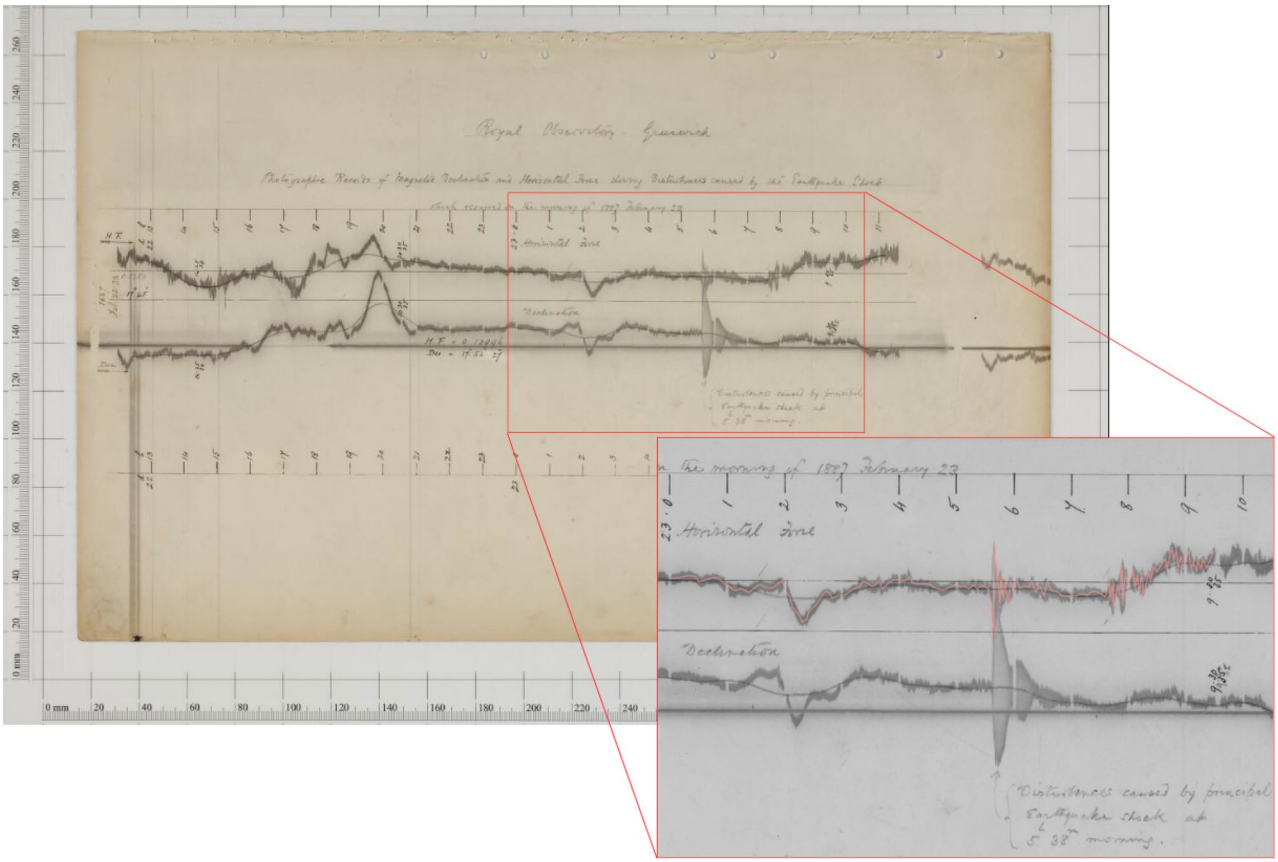

Fig. 1. Horizontal-force (H) and declination (D) traces recorded by the magnetometer at the Greenwich observatory, capturing variations in the Earth's magnetic field. Notably, the original annotations from 1887 highlight the disturbances caused by the Ligurian earthquake on 23 February. The enlarged section emphasizes the exact time at which the seismic waves, referred to as "disturbances," were detected (5:38 a.m.). The red trace represents the part of the signal that was digitized (see "Magnetogram digitization" section for more details) and subsequently used for all further analyses. Reproduced with the permission of the BGS ©*UKRI 2025*© *NERC 2025. All rights reserved.*.

The first attempt to discuss the mechanical effects of seismic waves on compass-needles dates back to Davison[40]. Liznar[52] and Reid[41] then formulated the first mathematical solutions for magnetic instruments employing unifilar and bifilar suspended magnets. The first one was used to record the local declination of the geomagnetic field, while the second one was used to record the local horizontal force. Eleman later provided a direct derivation of the response of these types of magnetometers to seismic waves[42]. Both types of magnetometers were characterized by two different oscillation periods, i.e. the natural pendulum period of the magnet system—due to the mass attached to the fiber—and the magnetic oscillation period. D and H instruments reacted differently to the north–south and east–west components of ground motion, exhibiting different sensitivities[42]. While the D bar magnets were aligned in the direction of the local declination of the geomagnetic field, the H bar magnets were aligned orthogonally to the magnetic meridian. The rotations of the D magnet resulted from the ground motion component orthogonal to the D direction, so that the declinometer functioned as a slightly misaligned east–west component, while the H instrument functioned as a slightly misaligned north–south component[44].

Methods

Magnetogram digitization

Although recovering seismic information contained in old records such as magnetometer traces is not an easy task, the quality of the scanned images was good enough to perform the digitization on every magnetometer record. The digitization process involved extracting the sample sequence directly from the image. The horizontal and vertical coordinates (x, y) were then converted into time and amplitude scales. This was only possible after having selected a reference system and taken into account the length of the minute and the line spacing on the original magnetogram[53]. For each magnetogram, the length of the time window used for digitization was variable and depended on the duration and quality of the traces. In the first step, the digitization was performed manually, trying to insert as many points as possible to follow the course of the traces. Then, starting from the scattered points, it was possible to automatically resample the signals with a fixed sampling step specific to each trace, varying according to the length and quality of the traces themselves. In any case, the exploitable frequency band

Fig. 2. Map showing the locations of the Greenwich magnetic observatories considered in this study (indicated by light blue triangles) as well as the estimated epicenter of the 1887 Ligurian earthquake (marked by a red star).

was restricted to an upper limit of just 0.03 Hz. In particular, the traces recorded at the Greenwich observatory were resampled at a fixed interval of 22 seconds. Similarly, the data from Falmouth was resampled at an interval of 16.7 seconds, while the traces from Kew were resampled every 22.5 seconds. The longest sampling step was performed for the Paris Saint-Maur observatory, where the data was resampled every 29 seconds.

Instrument response

To perform the instrument correction, we adhere to the theory of Eleman[42], which explains the response (T_{mag}) of a classical declinometer and/or a H instrument to harmonic ground displacement:

$$T_{mag} = \frac{M \times Z \times \omega^2 \times \exp\left[i \times (-\delta_1 - \delta_2)\right]}{I \times L \times \sqrt{\left(\omega_P^2 - \omega^2\right)^2 + \left(\frac{\alpha}{m}\right)^2 \times \omega^2} \times \sqrt{\left(\omega_M^2 - \omega^2\right)^2 + \left(\frac{\beta}{I}\right)^2 \times \omega^2}}, \tag{1}$$

in which ω_P and ω_M are the mechanical and magnetic eigenfrequencies of the magnetometer respectively, M is the magnetization of the bar magnet, Z is the magnetic field strength, I is the moment of inertia of the bar magnet, and L is its length, m is the mass of the magnet, α and β are the mechanical and magnetic damping constants. The phase shifts δ_1 and δ_2 are given by $\delta_1 = \arctan\left(\frac{\alpha}{m} \times \frac{\omega}{\omega_P^2 - \omega^2}\right)$ and $\delta_1 = \arctan\left(\frac{\beta}{I} \times \frac{\omega}{\omega_M^2 - \omega^2}\right)$, respectively. The far-field ground displacement $u_i\left(\underline{x}, t\right)$ resulting from a seismic point source, which is characterized by the moment tensor M_{jk}, is mathematically expressed as the convolution ($*$) of the time derivative of M_{jk} with the Green's function G_{ij} and the k-th component of the slowness vector s_k ([54,55]):

$$u_i\left(\underline{x}, t\right) = \dot{M}_{jk} * G_{ij} \times s_k. \tag{2}$$

In the frequency domain, the response of the magnetometer $\theta_i\left(\omega\right)$ is obtained by applying the transfer function of the instrument T_{mag} to the Fourier transform of the ground displacement $u_i\left(\underline{x}, t\right)$, which results in the equation:

$$\theta_i\left(\omega\right) = T_{mag} \times u_i\left(\underline{x}, t\right) = T_{mag} \times i \times \omega \times M_{jk} \times g_{ij} \times s_k, \tag{3}$$

in which g_{ij} represents the Fourier transform of the Green's function[44]. Following the methodology outlined by Eleman, $\frac{\beta}{I} = \frac{\alpha}{m} = 2 \times \varepsilon$ and the damping factor ε was assumed to be 0.0218 for the H component and 0.01832 for the D component of the magnetometers[42,56]. The absolute magnification of the instruments was neglected in order to focus exclusively on the relative response to the true ground displacement of the earthquake. The transfer function shows two peaks at the magnetic and mechanical eigenfrequencies, each associated with 180° phase shifts; it can be found in Fig. S34 in the Supplementary Information.

Cross-correlation analysis

To determine which seismic phases are actually observable on the digitized magnetograms, we selected the magnetic H trace recorded at the Greenwich observatory. This record was preferred due to its superior clarity and data quality after digitization (in this regard, Figures S1–S3 clearly show that the signals recorded at the other magnetic observatories are much fainter and significantly more difficult to interpret). To this end, we performed extensive tests using QSEIS[57] to compute synthetic full-wavefield seismograms for different fault scenarios, which we adopted from those proposed and tested by Larroque et al.[22]. The Green's functions were calculated based on the AK135 global seismic velocity model[58]. For our simulations, we considered pure thrust and normal faulting configurations (i.e., with a rake of $\pm 90^\circ$) and a latitude of 43.74°N, a longitude of 7.94°E, and a depth of 15 km for the source centroid (Fig. 5). The traces were simulated at equispaced epicentral distance steps up to 9.40°, which corresponds to the angular distance between the assumed source centroid location and the Greenwich magnetic observatory. For all simulations, we considered the static seismic moment (M_0) for a 6.8 M_w source, since considering different M_0 values does not lead to different shapes of the seismograms, but only causes an increase or a decrease in the amplitude of the simulated waveforms.

The simulated velocigrams were first integrated to obtain displacement seismograms and then bandpass filtered in the frequency range 0.006–0.01 Hz. The transfer characteristic of the magnetometer was then convolved with the simulated ground motion traces. We necessarily had to consider synthetic ground displacements up to periods of only 100 seconds for our analysis, as we found that the convolution of the instrument response tends to become highly unstable for longer periods. We scaled the synthetic signals with respect to the magnetogram based on their Fourier amplitude spectra differences evaluated at each point. For each simulated magnetometer trace, we calculated the cross-correlation with respect to the digitized magnetometer record to determine which time lag (i.e., temporal offset) yielded the highest value of the Pearson correlation coefficient, PCC (i.e., maximized the cross-correlation between the two time series), and then aligned the traces. Given two discrete signals $x = (x_1, \ldots, x_n)$ and $y = (y_1, \ldots, y_n)$, the PCC is defined as:

$$\rho_{xy} = \frac{\sum_{i=1}^{n}(x_i - \bar{x})(y_i - \bar{y})}{\sqrt{\sum_{i=1}^{n}(x_i - \bar{x})^2}\,\sqrt{\sum_{i=1}^{n}(y_i - \bar{y})^2}}, \tag{4}$$

in which $\bar{x}$ and $\bar{y}$ denote the mean values of x and y, respectively.

To further validate the robustness of the analysis, we also calculated the standard Euclidean norm (L_2) and the "Manhattan distance" (or "Taxicab norm," L_1) of the residuals between the two signals. For a given time lag τ, the residual vector is $r_i(\tau) = x_i - y_{i+\tau}$. The norms are defined as:

$$L_1(\tau) = \sum_{i=1}^{n} |r_i(\tau)|, \qquad L_2(\tau) = \sqrt{\sum_{i=1}^{n} r_i(\tau)^2}. \tag{5}$$

The optimal alignment corresponds to the lag τ that maximizes ρ_{xy} and, equivalently, minimizes both L_1 and L_2.

Magnitude calculation

The possibility of using magnetometer data to derive the magnitude of strong historical seismic events has already been demonstrated by Krüger et al.[44,59], who successfully derived M_w estimates for earthquakes in Central Asia that occurred in the late 19th century.

To derive a plausible magnitude estimate for the 1887 Ligurian earthquake, the M_w 6.10 earthquake in Emilia (Po Plain, northern Italy) on 20 May 2012 at 02:03:52 was chosen as a reference[60] (Fig. 3). We convolved the ground motion data recorded at the modern broadband station SWN1 in England (FDSN network code GB) with the transfer function of the magnetometer in order to simulate magnetograms for the 2012 Emilia event. This station was selected because both its source-receiver azimuth and epicentral distance are comparable to those between the 1887 Ligurian earthquake estimated hypocenter and the magnetic observatory of Greenwich. This analysis was restricted to Greenwich, as it is the only observatory for which digitized magnetometer records are available for both the D and H components, so that the magnitude can be calculated as the average of the two individual measurements.

Under the assumption of consistent Green's function characteristics—i.e., that the earthquakes compared occurred in the same region and exhibited similar focal mechanisms—it is expected that the magnetogram amplitude ratios scale proportionally to the ground motion amplitude ratios. This implies that they are also proportional to the moment rate ($\dot{M}_0$) ratio of the events. In addition, if the dominant periods observed in the magnetogram signals exceed the source corner frequencies, this proportionality can also be extended to the static seismic moment, M_0[44]. Therefore, assuming that the transfer characteristics of the recording instruments remain stable over time, the following linear relationship between the observed amplitudes of the D and H components and M_0 can be established, allowing consistent M_0 estimates based on magnetogram data:

$$\left[\frac{A^{(i)}}{A^{(ref)}}\right]_{c=D,H} = \left[\frac{M_0^{(i)}}{M_0^{(ref)}}\right]. \tag{6}$$

In this formulation, the term $A^{(i)}/A^{(ref)}$ represents the ratio between the magnetogram amplitude $A^{(i)}$ of the event i with unknown M_0 and the magnetogram amplitude $A^{(ref)}$ of the reference earthquake, both

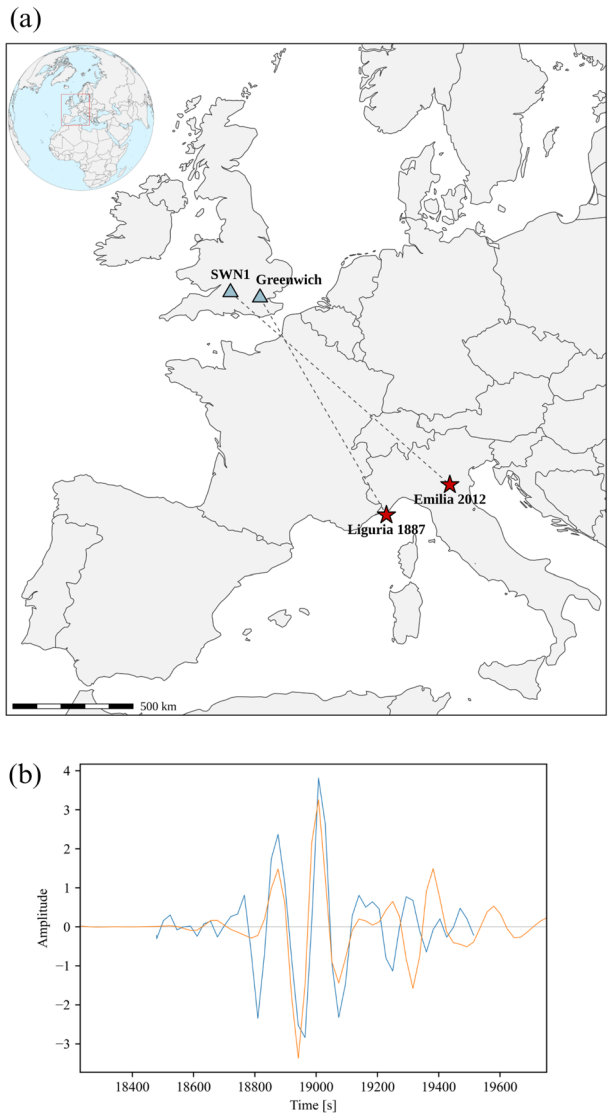

Fig. 3. (**a**) Map showing the locations of the Greenwich magnetic observatory and the broadband seismic station GB.SWN1 (indicated by light blue triangles), as well as the estimated epicenters of the 1887 Ligurian earthquake and the 2012 Emilia earthquake (marked by red stars). (**b**) Superposition between the simulated magnetometer trace for the 20 May 2012 M_w 6.10 Emilia earthquake recorded at GB.SWN1 (blue trace) and the digitized H magnetogram recorded at the magnetic observatory in Greenwich (orange trace). The synthetic Emilia magnetogram is scaled with respect to the Greenwich magnetogram based on the difference in their Fourier amplitude spectra.

measured on the same magnetometer component *c*. When expressed in logarithmic terms, this relationship can be reformulated as follows:

$$log\left(A^{(i)}\right) - log\left(A^{(ref)}\right) = log\left(M_0^{(i)}\right) - log\left(M_0^{(ref)}\right), \tag{7}$$

which can then be rearranged to yield an expression for the M_w of the analyzed event:

$$M_w^{(i)} = \frac{2}{3} \times \left[log\left(A^{(i)}\right) - log\left(A^{(ref)}\right)\right] + M_w^{(ref)}. \tag{8}$$

Results

Taking into account the complex seismotectonic and geological setting of the Liguria region, this study aims to clarify two important open questions about the 1887 earthquake: the estimation of its magnitude and the characterization of the focal mechanism. We do not address the location of the event, for which we rely on estimates from previous studies[22]. We examined all available scanned magnetograms in search of observable

seismic waveforms. We then digitized the scanned images and computed synthetic full-wavefield seismograms for different fault scenarios (Fig. 4a) adopted from recent literature[22]. The rupture parameters for the tested source geometries can be found in Table 1. We then processed the traces and performed the cross-correlation analysis, as described in the "Methods" section. Despite the fact that the bandwidth of the simulated magnetometer traces is obviously limited, we can verify how different phases—i.e., primary and secondary body waves—can nevertheless be identified (Fig. 4b).

The calculated PCC values are shown in Table 1. Scenarios 1, 2, 5 and 6 exhibit a more than satisfactory similarity between the modeled seismograms and the observed magnetogram (S1—PCC = 0.658; S2—PCC = 0.733; S5—PCC = 0.647; S6—PCC = 0.710) while the correlation is lower for scenarios 3 (PCC = 0.570) and 4 (PCC = 0.558). To further validate the robustness of the analysis, we also calculated the L_1- and L_2-norms and found in both cases best fitting (i.e., residuals minimizing) solutions in correspondence of the same time lags, thus obtaining comparable results (Supplementary Figs. S4–S9).

As previously mentioned, the H magnetogram recorded at Greenwich was preferred due to its higher quality; however, the same analysis was also performed for all other H and D available traces. The results can be found in the Supplementary Information in Figs. S10–S33 while the resulting PCC values are summarized in Table 2, together with the PCC results relative to the H trace recorded at Greenwich.

Regarding the magnitude calculation, applying Eq. 8 to the digitized and processed traces recorded at the magnetic observatory in Greenwich resulted in the M_w estimates presented in Table 3. The analysis was, in fact, limited to Greenwich, the only observatory with digitized magnetometer records for both the D and H components, allowing the magnitude to be calculated as the average of the two measurements. The averaging of the individual H and D M_w values for the magnetic observatory of Greenwich resulted in a M_w value of 7.233. Due to the limited number of available recordings, no estimates of the uncertainty associated with the magnitude calculation were derived.

Discussion

The response of magnetometers equipped with suspended magnets to seismic events has long been the subject of scientific debate. Interpretations have varied, with some attributing the observed disturbances to transient electromagnetic or magnetic oscillations induced by the earthquake, while others have argued in favor of a mechanical origin, involving the physical shaking of the instruments[47]. Notably, Eleman showed that pendulum-like motions of suspended magnets can generate magnetic torques, suggesting that magnetometers could react as ultra–low-sensitivity seismic recording devices[42]. Therefore, in exceptional cases, "seismomagnetic waves" could actually be observed. Although it is now generally accepted that standard magnetometers reacted primarily mechanically[44], it remains plausible that seismic waves could also have induced minor real magnetic disturbances.

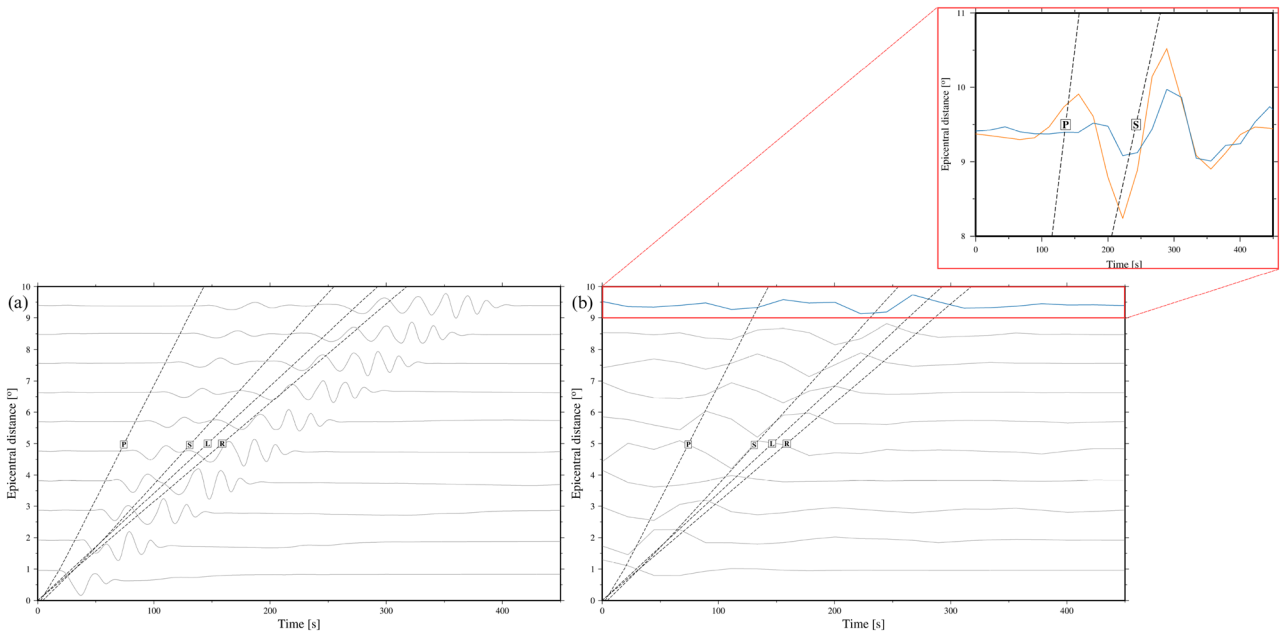

Fig. 4. (**a**) Synthetic full-wavefield seismograms for scenario S1 described in the text. (**b**) Simulated seismograms after integration, bandpass filtering and convolution with the magnetometer response, as described in the text. The inset shows the superposition between the processed synthetic seismogram (blue trace) and the digitized H magnetogram recorded at Greenwich (orange trace). In all figures, the traces are conspicuously vertically exaggerated. The dashed lines represent the travel times of body waves (primary, P; secondary, S) and surface waves (Rayleigh, R; Love, L) according to the AK135 seismic reference model.

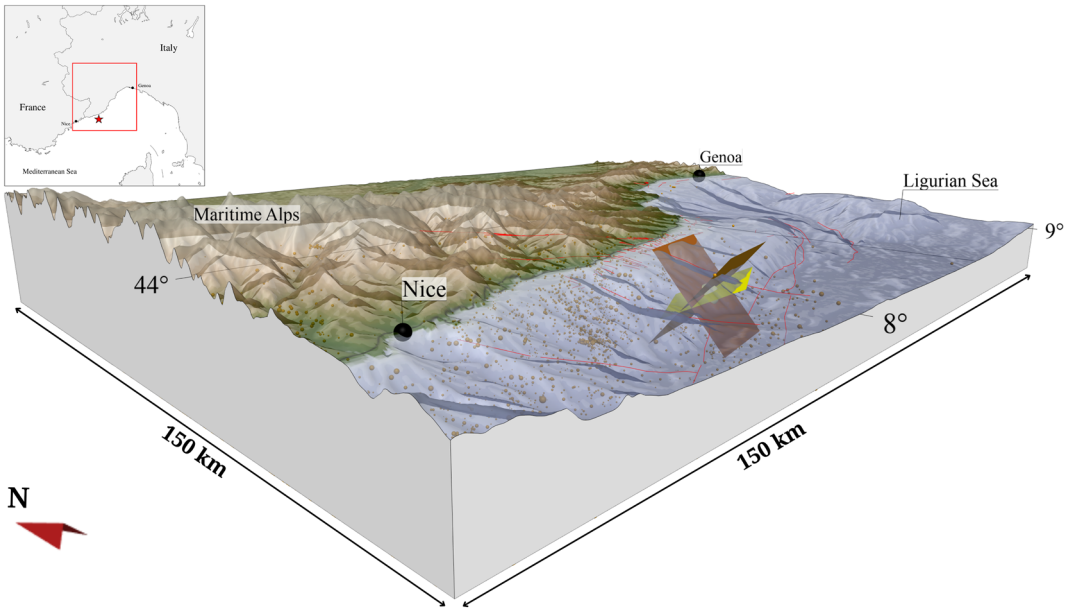

Fig. 5. Overview of the study area showing the offshore hypocenter of the Ligurian earthquake of 1887 (43.74°N latitude, 7.94°E longitude) and the three fault planes discussed in the text, for which the simulation of synthetic seismograms was carried out. The displayed hypocenter and fault planes have been shifted upwards for the sake of clarity, so that the depth of the hypocenter does not correspond to the actual depth used in the simulations (15 kilometers). The 235°–striking 16°–dipping northward plane (in yellow) indicates the one corresponding to the best-fitting scenario S1 (Table 1). The locations of the cities of Nice (France) and Genoa (Italy) are shown. The orange dots represent seismic events with magnitude values in the M_L range 0.1–4.1 that occurred in the region between 1 January 1985 and 1 August 2025. The red arrow in the lower left corner indicates the direction of the geographic north. The figure is sensibly exaggerated vertically so that the bottom of the three-dimensional model lies at a depth of 5 km. The topographic and bathymetric terrain models are from the GEBCO 2024 Grid (https://doi.org/10.5285/1c44ce99-0a0d-5f4f-e063-7086abc0ea0f), while the main tectonic elements (red lines) are from the Geological Survey of Italy (https://www.isprambiente.gov.it). The hypocenters of the earthquakes are derived from the Istituto Nazionale di Geofisica e Vulcanologia (INGV) catalog (https://terremoti.ingv.it). The figure was created using QGIS 3.34.8 (http://www.qgis.org) .

Scenario	Kinematics	Strike	Dip	PCC
S1	Reverse	235°	16°N	0.658
S2	Normal	235°	16°N	0.733
S3	Reverse	250°	70°N	0.570
S4	Normal	250°	70°N	0.558
S5	Reverse	70°	70°S	0.647
S6	Normal	70°	70°S	0.710

Table 1. The scenarios discussed in the text for the 1887 Ligurian earthquake, with fixed source centroid location (7.94°E, 43.74°N) and focal depth (15 km). The rake angle is adjusted to account for both pure reverse and normal faulting (i.e., with a rake of ±90°). The strike and dip angles are reported together with the Pearson correlation coefficient (PCC) values calculated for each fault scenario relative to the H trace recorded at the Greenwich observatory.

The results of the cross-correlation analysis carried out for the Greenwich H trace show that scenarios 1, 2, 5 and 6 (Table 1) exhibit a high degree of similarity between the modeled seismograms and the observed magnetogram. This significantly confirms the robustness of the selected fault scenarios previously proposed and validated by Larroque et al. based on macroseismic data and tsunami characteristics[22]. The PCC values obtained across the different observatories also indicate a general coherence in the results (Table 2), although variations in the quality of the magnetograms—particularly those with lower resolution or more ambiguous signal characteristics—may substantially influence the reliability of the analysis. Despite these limitations, the results provide additional support for the robustness of the preferred fault scenarios.

However, the interpretation of focal mechanisms based solely on seismological data is inherently ambiguous, as it does not allow for a definitive distinction between the actual fault plane and the auxiliary plane. Scenarios

	PCC				
Scenario	Greenwich (H)	Greenwich (D)	Kew (H)	Falmouth (H)	Paris Saint-Maur (D)
S1	0.658	0.579	0.494	0.521	0.378
S2	0.733	0.604	0.458	0.389	0.469
S3	0.570	0.371	0.391	0.581	0.494
S4	0.558	0.425	0.351	0.553	0.456
S5	0.647	0.583	0.518	0.321	0.380
S6	0.710	0.589	0.488	0.301	0.455

Table 2. PCC values calculated for each fault scenario by comparing the synthetic convolved seismograms with the D and H magnetograms recorded at Greenwich, the D magnetogram recorded at Paris, and the H magnetograms recorded at Kew and Falmouth.

Station	Component	M_w
Greenwich	H	7.045
Greenwich	D	7.420

Table 3. Estimated M_w values for the 1887 Ligurian earthquake based on magnetogram amplitudes recorded at the Greenwich magnetic observatory. The values were obtained independently from the H and D components using Eq. 8. The average of the two estimates yields a final M_w of 7.233.

1 and 2 assume a fault plane oriented at 235° with a dip of 16° to the north, whereas scenarios 5 and 6 refer to a plane striking at 70° and dipping 70° to the south, approximately corresponding to the auxiliary plane of the first configuration. While scenarios 5 and 6 result in slightly higher PCC values, the overall cross-correlation values for all four scenarios are of a comparable magnitude. However, considering the geological and structural context of the southwest Alps–Ligurian Basin junction—which is essentially characterized by predominantly reverse offshore north-dipping fault systems parallel to the coastline and extensional structures along the upper continental slope[19,21,34,61,62]—the reverse-kinematics fault plane described in scenario S1 proves to be the most plausible solution (Table 1). The spatial distribution of recent onshore and offshore seismicity, showing mainly diffuse patterns and exhibiting predominantly compressional and transpressional focal mechanisms[9,10,16,18–20], and the tide gauge record modeling for the tsunami generated by the earthquake provide further evidence. In particular, Larroque et al.[22] and Ioualalen et al.[63] have demonstrated that normal faulting scenarios are not in accordance with tsunami modeling, as they do not satisfy the polarity of the observed first arrival wave in the Genoa harbor. It is worth noting, nevertheless, that over time various authors have proposed different interpretations regarding the fault responsible for the 1887 Ligurian earthquake, such as in the case of Eva and Rabinovich[28], who postulated that the event was caused by the activation of a normal fault, in stark contrast to the results of the French authors.

Whilst acknowledging that the analysis presented inevitably entails a significant qualitative component—especially in the subjective selection of the signal portion used to calculate the cross-correlation coefficient—and is therefore subject to inherent limitations, we believe that it can nevertheless provide valuable insights and make an additional contribution to the understanding of the 1887 Ligurian earthquake. The results confirm that seismic hazard models for the region should consider a compressive stress regime, with the 1887 Ligurian earthquake likely caused by the activation of a low-angle north-dipping reverse fault.

The identification of primary and secondary body waves within the limited bandwidth of the magnetograms emphasizes the ability of historical magnetometers to record key seismic phases, despite their limitations. In addition to fault characterization, we provided a direct M_w estimate of the earthquake based on magnetometer data , using a recent M_w 6.10 earthquake in Emilia as a reference (Fig. 3). Although it is highly unlikely that this event released an amount of energy comparable to the 1887 earthquake, it represents the only recent earthquake with strong and reliable ground motion recordings that occurred sufficiently close to the study area (i.e., its azimuth and epicentral distance with respect to the magnetic observatories in the UK and France are essentially comparable). The epicentral distance between the two events is indeed less than 300 km, which constitutes a reasonable approximation for the purposes of our analysis. This result is particularly significant given the scarcity of reliable instrumental observations and the previous lack of analysis of recorded data for the 1887 Ligurian earthquake. It highlights the potential of digitized magnetograms to contribute to the quantitative re-evaluation of major pre-instrumental events, offering valuable constraints for seismic hazard assessments. Modern analytical techniques can further enhance the utility of these records and facilitate the reconstruction of seismic and geodynamic processes at both regional and local scales. This is particularly valuable for regions with low-to-moderate seismic activity, where seismogenic sources may have medium- to long-term recurrence intervals.

Data availability

Any request of magnetogram data should be directly addressed to the British Geological Survey and the Bureau Central de Magnétisme Terrestre. The datasets used and/or analyzed during the current study are available from the corresponding author upon reasonable request.

Received: 27 June 2025; Accepted: 24 October 2025
Published online: 25 November 2025

References

1. Ferrari, G. The 1887 Ligurian earthquake: A detailed study from contemporary scientific observations. *Tectonophysics* **193**, 131–139. https://doi.org/10.1016/0040-1951(91)90194-W (1991).
2. Rovida, A., Locati, M., Camassi, R., Lolli, B. & Gasperini, P. The Italian earthquake catalogue CPTI15. *Bull. Earthq. Eng.* **18**, 2953–2984. https://doi.org/10.1007/s10518-020-00818-y (2020).
3. Rovida, A. et al. Italian Parametric Earthquake Catalogue (CPTI15), version 4.0. Istituto Nazionale di Geofisica e Vulcanologia (INGV). https://doi.org/10.13127/cpti/cpti15.4 (2022).
4. Davison, C. *A study of recent earthquakes* (The Walter Scott publishing co., ltd., London, 1905).
5. Taramelli, T. & Mercalli, G. *Il terremoto ligure del 23 febbraio 1887*. Estratto dagli Annali dell'Ufficio Centrale di Meteorologia e Geodinamica (Tip. Metastasio, 1888).
6. Dercourt, J. et al. Geological evolution of the Tethys belt from the Atlantic to the Pamirs since the LIAS. *Tectonophysics* **123**, 241–315. https://doi.org/10.1016/0040-1951(86)90199-X (1986).
7. Dewey, J., Helman, M., Knott, S., Turco, E. & Hutton, D. Kinematics of the western Mediterranean. *Geol. Soci. London, Special Publ.* **45**, 265–283. https://doi.org/10.1144/GSL.SP.1989.045.01.15 (1989).
8. Jolivet, L. & Faccenna, C. Mediterranean extension and the Africa-Eurasia Collision. *Tectonics* **19**, 1095–1106. https://doi.org/10.1029/2000TC900018 (2000).
9. Morelli, D. et al. Morpho-Structural Setting of the Ligurian Sea: The Role of Structural Heritage and Neotectonic Inversion. *J. Mar. Sci. Eng.* https://doi.org/10.3390/jmse10091176 (2022).
10. Béthoux, N. et al. A closing Ligurian Sea?. *Pure Appl. Geophys.* **139**, 179–194. https://doi.org/10.1007/BF00876326 (1992).
11. Ritz, J.-F. Tectonique récente et sismotectonïque des Alpes du Sud: Analyses en termes de contraintes. *Quaternaire* **3**, 111–124. https://doi.org/10.3406/quate.1992.1980 (1992).
12. Sébrier, M., Ghafiri, A. & Bles, J.-L. Paleoseismicity in France: Fault trench studies in a region of moderate seismicity. *J. Geodyn.* **24**, 207–217. https://doi.org/10.1016/S0264-3707(97)00005-7 (1997).
13. Eva, E. & Solarino, S. Variations of stress directions in the western Alpine arc. *Geophys. J. Int.* **135**, 438–448. https://doi.org/10.1046/j.1365-246X.1998.00649.x (1998).
14. Baroux, E., Béthoux, N. & Bellier, O. Analyses of the stress field in southeastern France from earthquake focal mechanisms. *Geophys. J. Int.* **145**, 336–348. https://doi.org/10.1046/j.1365-246X.2001.01362.x (2001).
15. Larroque, C. et al. Active and recent deformation at the Southern Alps - Ligurian basin junction. *Netherlands J. Geosci.* https://doi.org/10.1017/S0016774600023878 (2001).
16. Larroque, C., Delouis, B., Godel, B. & Nocquet, J.-M. Active deformation at the southwestern Alps-Ligurian basin junction (France-Italy boundary): Evidence for recent change from compression to extension in the Argentera Massif. *Tectonophysics* **467**, 22–34. https://doi.org/10.1016/j.tecto.2008.12.013 (2009).
17. Barani, S., Scafidi, D. & Eva, C. Strain rates in northwestern Italy from spatially smoothed seismicity. *J. Geophys. Res.* https://doi.org/10.1029/2009JB006637 (2010).
18. Scafidi, D. et al. Seismicity of Northwestern Italy during the last 30 years. *J. Seismol.* https://doi.org/10.1007/s10950-014-9461-0 (2015).
19. Sage, F. et al. Structure and evolution of a passive margin in a compressive environment: Example of the south-western Alps-Ligurian basin junction during the Cenozoic. *Mar. Petrol. Geol.* **28**, 1263–1282. https://doi.org/10.1016/j.marpetgeo.2011.03.012 (2011).
20. Fanucci, F. & Morelli, D. *Rapporti tra morfologia e tettonica sul Margine Continentale Ligure*. Contributi al meeting marino 25–26 ottobre 2012 pp. 53–57 (D'Angelo, S. and Fiorentino, A., Eds., Atti ISPRA, Roma, 2013).
21. Morelli, D. et al. Geohazard features of the Ligurian Sea. *J. Maps* **20**, 2342920. https://doi.org/10.1080/17445647.2024.2342920 (2024).
22. Larroque, C., Scotti, O., Ioualalen, M., Hassoun, V. & Migeon, S. Reappraisal of the 1887 Ligurian earthquake (western Mediterranean) from macroseismicity, active tectonics and tsunami modelling. *Geophys. J. Int.* **190**, 8111. https://doi.org/10.1111/j.1365-246X.2012.05498.x (2012).
23. Reiter, L. *Earthquake Hazard Analysis: Issues and Insights* (Columbia Univ. Press, 1990).
24. Cornell, C. A. Engineering seismic risk analysis. *Bull. Seismol. Soc. Am.* **58**, 1583–1606. https://doi.org/10.1785/BSSA0580051583 (1968).
25. Capponi, G., Cattaneo, M. & Merlanti, F. *The Ligurian earthquake of February 23, 1887*. Atlas of Isoseismal Maps of Italian Earthquakes (Postpischl, D., Ed., CNR-PFG, Quaderni della Ricerca Scientifica, 114, 2A, Consiglio Nazionale delle Ricerche, Roma, 1990).
26. Tinti, S., Vittori, T. & Mulargia, F. On the macroseismic magnitudes of the largest Italian earthquakes. *Tectonophysics* **138**, 159–178. https://doi.org/10.1016/0040-1951(87)90037-0 (1987).
27. Boschi, E. Catalogo. et al. *(Istituto Nazionale di Geofisica-Storia Geofisica Ambiente* 1995 (ING-SGA, Bologna, 1980).
28. Eva, C. & Rabinovich, A. The February 23, 1887 tsunami recorded on the Ligurian Coast, western Mediterranean. *Geophysical Research Letters - GEOPHYS RES LETT* **24**, 2211–2214. https://doi.org/10.1029/97GL02110 (1997).
29. Guidoboni, E. et al. CFTI5Med, Catalogo dei Forti Terremoti in Italia (461 a.C.-1997) e nell'area Mediterranea (760 a.C.-1500) - Istituto Nazionale di Geofisica e Vulcanologia (INGV). https://doi.org/10.6092/ingv.it-cfti5 (2018).
30. Lagomarsino, S. *GNDT – Western Liguria project: Objectives, results and products* (Proc. of the Italian Conference on Seismic Risk, Built-up environment and Historical Centers, Sanremo, Italy, 2005).
31. Locati, M. et al. Italian Macroseismic Database (DBMI15), version 4.0, data sets. Istituto Nazionale di Geofisica e Vulcanologia (INGV),.https://doi.org/10.13127/dbmi/dbmi15.4 (2022).
32. Scotti, O., Baumont, D., Quenet, G. & Levret, A. The French macroseismic database SISFRANCE: Objectives, results and perspectives. *Ann. Geophys.* **47**, 571–581. https://doi.org/10.4401/ag-3323 (2004).
33. Bakun, W. H. & Scotti, O. Regional intensity attenuation models for France and the estimation of magnitude and location of historical earthquakes. *Geophys. J. Int.* **164**, 596–610. https://doi.org/10.1111/j.1365-246X.2005.02808.x (2006).
34. Larroque, C., de Lépinay, B. & Migeon, S. Morphotectonic and fault-earthquake relationships along the northern Ligurian margin (western Mediterranean) based on high resolution, multibeam bathymetry and multichannel seismic-reflection profiles. *Mar. geophys. Res.* **32**, 163–179. https://doi.org/10.1007/s11001-010-9108-7 (2010).
35. Cecchi, P. F. Sismografo elettrico a carte affumicate scorrevoli. *Atti Accad. pontif. Nuovi Lincei* **29**, 421–428 (1876).

36. Denza, P. F. Osservazioni fatte all'Osservatorio di Moncalieri sul terremoto del 23 febbraio 1887. *Bollettino Mensuale pubblicato per cura dell'Osservatorio Centrale del Real Collegio Carlo Alberto in Moncalieri, Torino* **7**, 68–70 (1887).
37. Fouqué, F. *Les Tremblements de Terre* (Librairie J. B. Baillière et Fils, Paris, 1888).
38. Agamennone, G. *La Registrazione dei Terremoti* (Casa Editrice "L'Elettricista", 1906).
39. Dewey, J. & Byerly, P. The early history of seismometry (to 1900). *Bull. Seismol. Soc. Am.* **59**, 183–227 (1969).
40. Davison, C. IV-On a Possible Cause of the Disturbance of Magnetic Compass-Needles during Earthquakes. *Geol. Mag. (Decade III)* **2**, 210–211 (1885).
41. Reid, H. F. The free and forced vibrations of a suspended magnet: 1. *Theory. Terrestr. Magnet. Atmos. Electr.* **19**, 57–72. https://doi.org/10.1029/TE019i002p00057 (1914).
42. Eleman, F. The Response of Magnetic Instruments to Earthquake waves. *J. Geomag. Geoelectr.* **18**, 43–72. https://doi.org/10.5636/jgg.18.43 (1966).
43. Batlló, J., Arrazola, D. & Ugalde, A. Using magnetograms for earthquake magnitude evaluation. *Eos, Trans. Am. Geophys. Un.* **86**. https://doi.org/10.1029/2005EO480003 (2005).
44. Krüger, F., Kulikova, G. & Landgraf, A. Magnitudes for the historical 1885 (Belovodskoe), the 1887 (Verny) and the 1889 (Chilik) earthquakes in Central Asia determined from magnetogram recordings. *Geophys. J. Int.* **215**, 1824–1840. https://doi.org/10.1093/gji/ggy377 (2018).
45. Mascart, E. Remarques. & de M. Mascart au sujet de cette communication [Fines]. *C. R. Acad. Sci. Paris* **104**:606–608 (1887).
46. Offret, A. Tremblements de terre du 23 février 1887. Heures de l'arrivée des secousses en dehors de l'épicentre. *C. R. Acad. Sci. Paris* **104**, 1238–1242 (1887).
47. Poirier, J.-P., Perrier, F. & Le Mouël, J.-L. On some electrical effects of the 1887 Ligurian earthquake. *Comptes Rendus Geoscience* **340**, 203–210. https://doi.org/10.1016/j.crte.2007.12.004 (2008).
48. Malin, S. R. C. 150th anniversary of Gauss's first absolute magnetic measurement. *Nature* **297**. https://doi.org/10.1038/297285a0 (1982).
49. Malin, S. R. C. Sesquicentenary of Gauss's First Measurement of the Absolute Value of Magnetic Intensity. *Phil. Trans. R. Soc. Lond.* **306**, 5–8. https://doi.org/10.1098/rsta.1982.0060 (1982).
50. Malin, S. R. C. Geomagnetism at the Royal Observatory. *Greenwich. Q. J. R. Astr. Soc.* **37**, 65–74. https://doi.org/10.1038/297285a0 (1996).
51. BGS. Historical UK magnetic observatory magnetograms and yearbooks, British Geological Survey, http://www.bgs.ac.uk/data/Magnetograms/home.html, Last accessed on 1 May 2025. (2017).
52. Liznar, J. Einfluss des Erdbebens vom April 1895 auf die Magnetographen in Pola und Wien nebsteinigen Bemerkungen ber die Wirkung der Erdbeben auf magnetische Variationsapparate überhaupt. *Meteor. Zeitschrift* **12** (1895).
53. Sandron, D., Renner, G., Rebez, A. & Slejko, D. Early instrumental seismicity recorded in the eastern Alps. *Boll. Geof. Teor. Appl.* **55**, 755–788. https://doi.org/10.4430/bgta0118 (2014).
54. Aki, K. & Richards, P. G. *Quantitative Seismology* (University Science Books, 2002).
55. Dahm, T. Relative moment tensor inversion based on ray theory: Theory and synthetic tests. *Geophys. J. Int.* **124**, 245–257. https://doi.org/10.1111/j.1365-246X.1996.tb06368.x (2007).
56. Christie, W. H. M. Results of the Magnetical and Meteorological Observations Made at the Royal Observatory, Greenwich, in the Year 1887. *Greenwich Observations in Astronomy, Magnetism and Meteorology made at the Royal Observatory* **49** (1889).
57. Wang, R. A simple orthonormalization method for stable and efficient computation of Green's functions. *Bull. Seismol. Soc. Am.* **89**, 733–741. https://doi.org/10.1785/BSSA0890030733 (1999).
58. Kennett, B. L. N., Engdahl, E. R. & Buland, R. Constraints on seismic velocities in the earth from traveltimes. *Geophys. J. Int.* **122**, 108–124. https://doi.org/10.1111/j.1365-246X.1995.tb03540.x (1995).
59. Krüger, F., Kulikova, G. & Landgraf, A. Instrumental magnitude constraints for the 11, Chilik earthquake. *Geol. Soci., London, Special Publ.* **432**, 2015. https://doi.org/10.1144/SP432.8 (1889).
60. Saraò, A. & Peruzza, L. Fault-plane solutions from moment-tensor inversion and preliminary Coulomb stress analysis for the Emilia Plain. *Ann. Geophys.* https://doi.org/10.4401/ag-6134 (2012).
61. Bigot-Cormier, F. et al. Déformations pliocènes de la marge nord-Ligure (France): les conséquences d'un chevauchement crustal sud-alpin - Pliocene deformation of the north-Ligurian margin (France): consequences of a south-Alpine crustal thrust. *Bull. Soc. Géol. Fr.* **175**, 197–211 (2004).
62. Béthoux, N., Tric, E., Chery, J. & Beslier, M.-O. Why is the Ligurian Basin (Mediterranean Sea) seismogenic? Thermomechanical modeling of a reactivated passive margin. *Tectonics* https://doi.org/10.1029/2007TC002232 (2008).
63. Ioualalen, M., Larroque, C., Scotti, O. & Daubord, C. Tsunami Mapping Related to Local Earthquakes on the French-Italian Riviera (Western Mediterranean). *Pure Appl. Geophys.* https://doi.org/10.1007/s00024-013-0699-1 (2014).

Acknowledgements

The authors express their deepest gratitude to the British Geological Survey and the Bureau Central de Magnétisme Terrestre for providing magnetogram records.

Author contributions

S.P. laid out the project and retrieved the magnetograms. Denis S. digitized the recordings. G.T. conducted the analysis. G.T., S.P., and Daniele S. jointly analyzed and interpreted the results. G.T. drafted the manuscript and prepared the figures. All authors jointly finalized it.

Funding

This research received no external funding.

Declarations

Competing interests

The authors declare no competing interests.

Additional information

Supplementary Information The online version contains supplementary material available at https://doi.org/10.1038/s41598-025-25870-z.

Correspondence and requests for materials should be addressed to G.T.